Electronic Supplementary Information for:

Production of novel carbon nanostructures by electrochemical reduction of polychlorinated organic rings under mild conditions for supercapacitors

Züleyha Kudaş[a], Emir Çepni[b,c], Emre Gür[d] and Duygu Ekinci*[a]

[a]Department of Chemistry, Faculty of Sciences, Atatürk University, 25240 Erzurum. Turkey.

[b]Department of Nanoscience and Nanoengineering, Nanomaterials Sciences, Atatürk University, 25240 Erzurum, Turkey.

[c]Department of Electrical and Electronic Engineering, Faculty of Engineering, Atatürk University, 25240 Erzurum, Turkey.

[d]Department of Physics, Faculty of Sciences, Atatürk University, 25240 Erzurum. Turkey.

Corresponding author e-mail address: dekin@atauni.edu.tr

Table of Contents

ESI1. Electrochemical Reduction of Hexachlorocyclopentadiene (HCCP)

The electrochemical reduction behaviour of HCCP was investigated by cyclic voltammetry. Fig. S1 shows a typical cyclic voltammogram obtained in acetonitrile solution containing 2 mM HCCP and 0.1 M TBABF$_4$ at a gold electrode. As seen, the voltammogram exhibits a well-defined irreversible cathodic peak at -0.73 V followed by a series of small reduction peaks at -1.15, -1.47 and -1.86 V vs. Ag/AgCl/KCl (3.0 M).
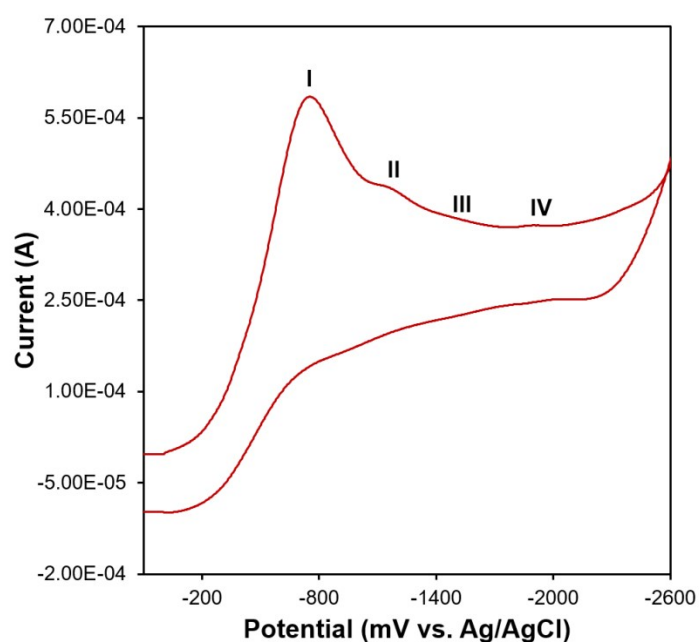

Fig. S1 Cyclic voltammogram of HCCP in acetonitrile containing 0.1 M TBABF$_4$. The scan rate is 0.1 V s^{-1}.

The electroreductive dehalogenation process of HCCP in aqueous buffer solution has been previously reported by Bedioui *et al.*[1] They noted that electrocatalytic reduction of HCCP at HOPG electrode modified with DDAB/Hemin surfactant film showed an irreversible cathodic wave with a peak potential of -1.10 V vs. SCE. This potential is significantly more negative than that observed in our experiments (-0.73 V vs. Ag/AgCl/KCl (3.0 M)). The significant positive shift in the reduction potential can associated with the catalytic effect of the gold electrode.[2]
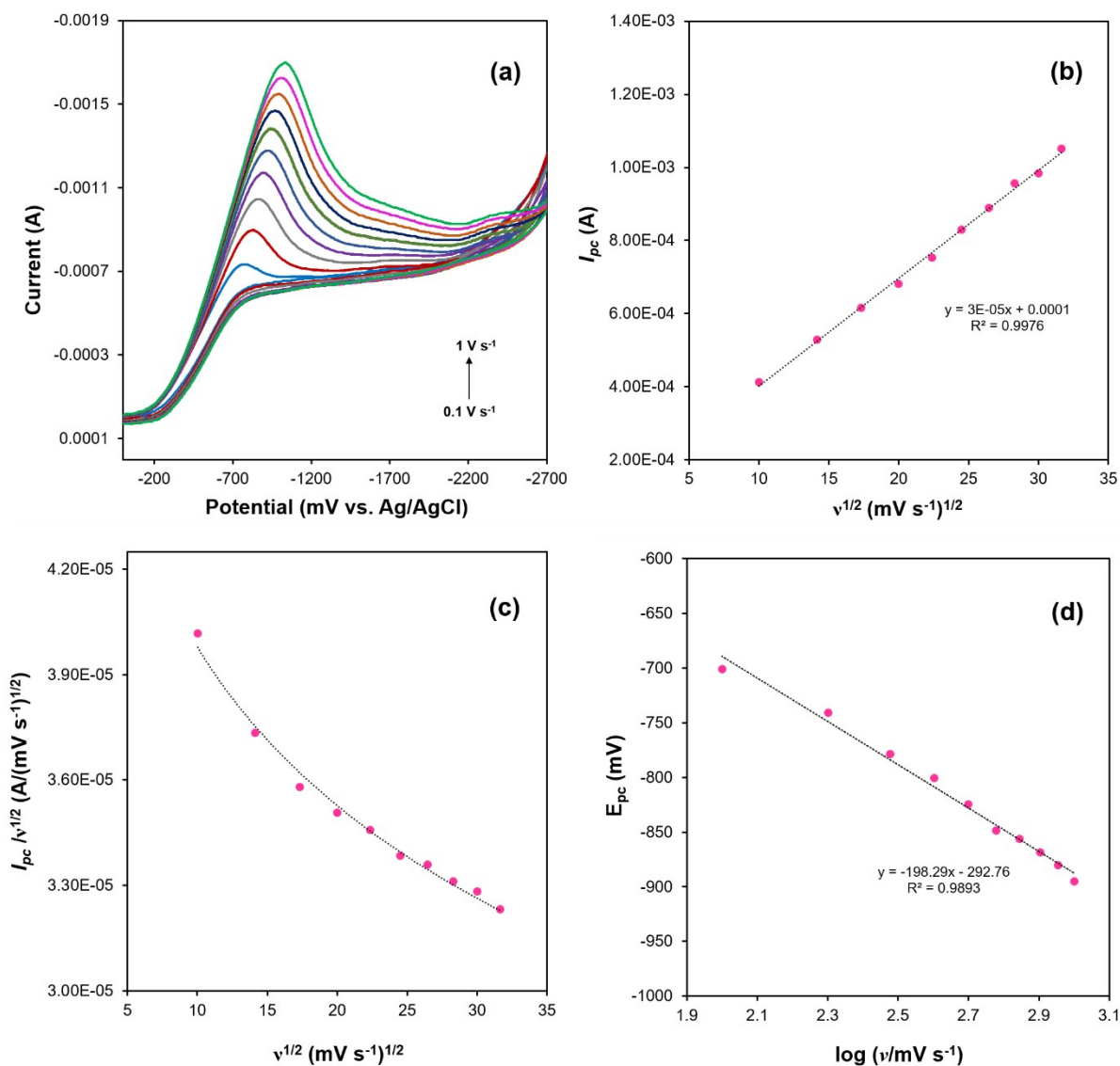
Fig. S2 (a) Cyclic voltammograms recorded at different scan rates in acetonitrile solution containing 2 mM HCCP and 0.1 M TBABF$_4$. (b) Variation of cathodic peak current with square root of scan rate for the first peak. (c) Variation of the current function (I$_{pc}$/v$^{1/2}$) with the square root of the scan rate (v$^{1/2}$) for the first peak. (d) Variation of the cathodic peak potential with the logarithm of scan rate for the first peak.

To further understand the electrochemical reduction behaviour of HCCP on gold electrodes, a series of the cyclic voltammograms were recorded at different scan rates (0.1-1.0 V s^{-1}) in acetonitrile solution containing 2 mM HCCP and 0.1 M TBABF$_4$ (Fig. S2a). As seen in Fig. S2a, the cathodic

peak currents increase as the scan rate is increased. In addition, the cathodic peak potentials shift to more negative potentials with increasing scan rate. For the first peak, the plot of the cathodic peak current (I_{pc}) versus the square root of the scan rate ($v^{1/2}$) is linear (Fig. S2b), and also the current function ($I_{pc}/v^{1/2}$) decrease with increasing $v^{1/2}$ (Fig. S2c). These observations indicate that the nature of redox process is diffusion controlled and electron transfer is followed by a chemical reaction.

In order to find the rate-determining step during the reduction process of HCCP, the electron transfer coefficient (α) was calculated from cyclic voltammograms using the variation of cathodic peak potential (E_{pc}) with logarithm of scan rate (log v) according to Eq. 1,

$$E_{pc} = -\frac{1.151RT}{\alpha F}logv$$

(1)

where R is the gas constant (8.314 J K^{-1} mol^{-1}); T is the room temperature (298 K) and F is the Faraday constant (96500 C mol^{-1}). Fig. S2d shows the variation of E_{pc} as a function of log v. From the slope of the graph, the α value was calculated to be 0.15 for HCCP, suggesting that electron transfer process is the rate-determining step, and thus that the reduction occurs through a concerted mechanism.[2-5]

To determine the number of electrons transferred (n) during the electrochemical reduction of HCCP, chronocoulometry experiments were performed. Experiments were conducted by applying potential steps from 0.0 V to -0.7 V and to -2.9 V vs. Ag/AgCl/KCl (3.0 M) in the time domain from 0.5 to 16 s. Fig. S3a shows representative chronocoulometry curves recorded by stepping the applied potential from 0.0 V to -2.9 V. As shown, the total charge (Q) gradually increases with time (t). Also, the Q values for both applied step potentials are linearly proportional to the value of $t^{1/2}$ (Fig. S3b). The n values were calculated from Q vs. $t^{1/2}$ plots using Anson equation (Eq.2),[6]

$$Q = \frac{2nFAC_0D^{1/2}}{\pi^{1/2}}t^{1/2}$$

(2)

where Q is the charge (C); n is the number of electrons transferred; F is Faraday's constant (96500 C mol^{-1}); A is the area of the working electrode; C_0 is the bulk concentration of HCCP (2×10^{-6} mol cm^{-3}) and D is diffusion coefficient (taken to be 1.0×10^{-5} cm^2 s^{-1}). Thus, the n values were found to be 4.5 and 12.4 for the step potentials of -0.7 V and -2.9 V vs. Ag/AgCl/KCl (3.0 M), respectively.
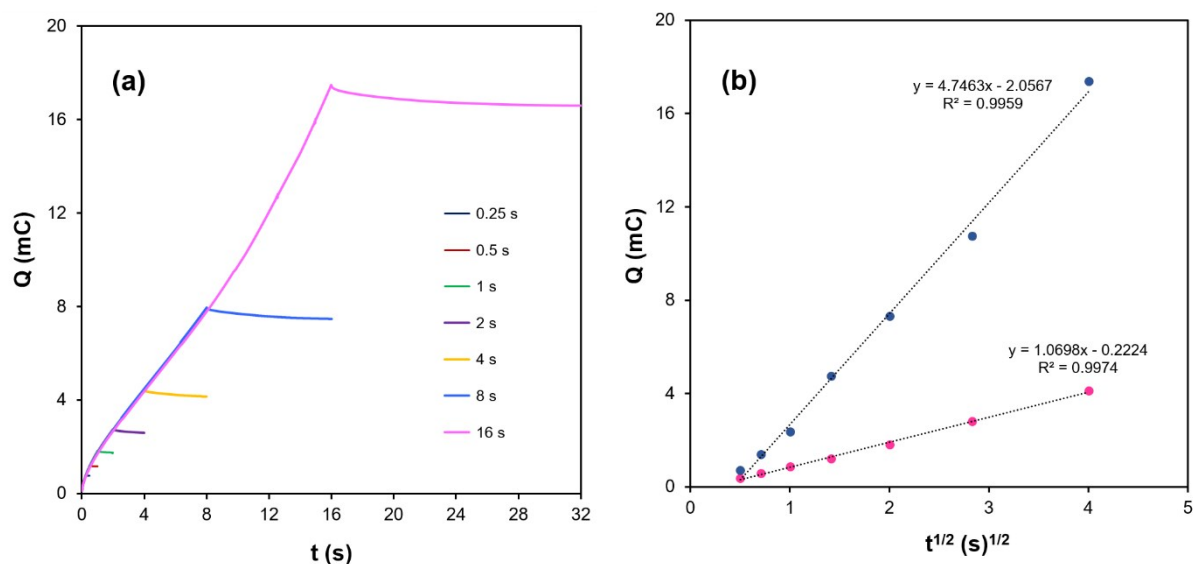

Fig. S3 (a) Chronocoulograms recorded in acetonitrile containing 2 mM HCCP and 0.1 M TBABF$_4$ at different time domains. The potential was stepped from 0.0 V to -2.9 V. (b) The plots of the total charge (Q) versus t$^{1/2}$ for HCCP at the same conditions. The potentials were stepped from 0.0 V to -0.7 V (•) and to -2.9 V (•).

The catalytic reduction of HCCP has been previously studied in the presence of metal and/or metal salts such as zinc, copper, copper chloride and tin chloride as reducing agents.[7-10] The HCCP is reduced in a stepwise manner to 1,2,3,4,5-pentachlorocyclopentadiene (PCCP) and 1,2,3,4-tetrachlorocyclopentadiene (TCCP) with zinc in HCl solution.[7,8] Since these molecules (PCCP and TCCP) can act both as dienes and dienophiles in the Diels-Alder reactions, they slowly undergoes cycloaddition with themselves to give [2.2.1]bicycloheptene derivatives under relatively mild conditions. Besides, HCCP is subjected to homogeneous bimolecular reductive coupling reaction by copper and copper chloride to yield bis-(pentachlorocyclopentaadienyl) (bis-PCCP).[9,10]

In this regard, to elucidate the nature of products obtained from the electrochemical reduction of HCCP, potential-controlled electrolysis experiments were conducted at -0.7 V and -2.9 V vs. Ag/AgCl/KCl (3.0 M) in acetonitrile solution containing 2 mM HCCP and 0.1 M TBABF$_4$. After electrolysis for 2 h, electrolyte solutions were analysed by Q-TOF LC/MS (Fig. S4). As shown, the mass spectra display two prominent peaks at m/z 242.28 and 571.59 as well as several lower intensity peaks at higher masses. The peak at m/z 242.28 is the molecular ion peak caused by the cation of the TBABF$_4$.[11] The prominent peak at m/z 571.59 and other small peaks in the spectra can be attributed to the [2.2.1]bicycloheptene structures produced by Diels-Alder cycloaddition reactions of cyclopentadiene derivatives generated during electrolysis.[12-14]
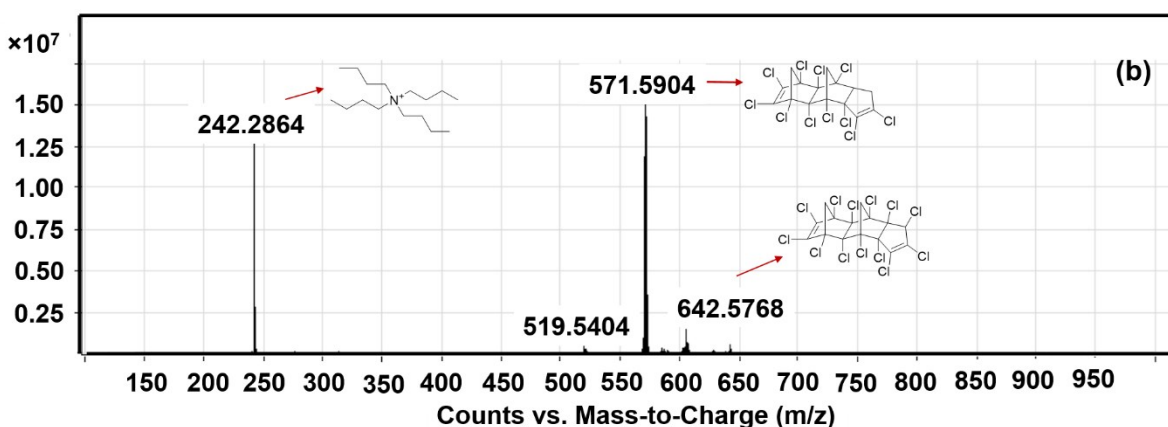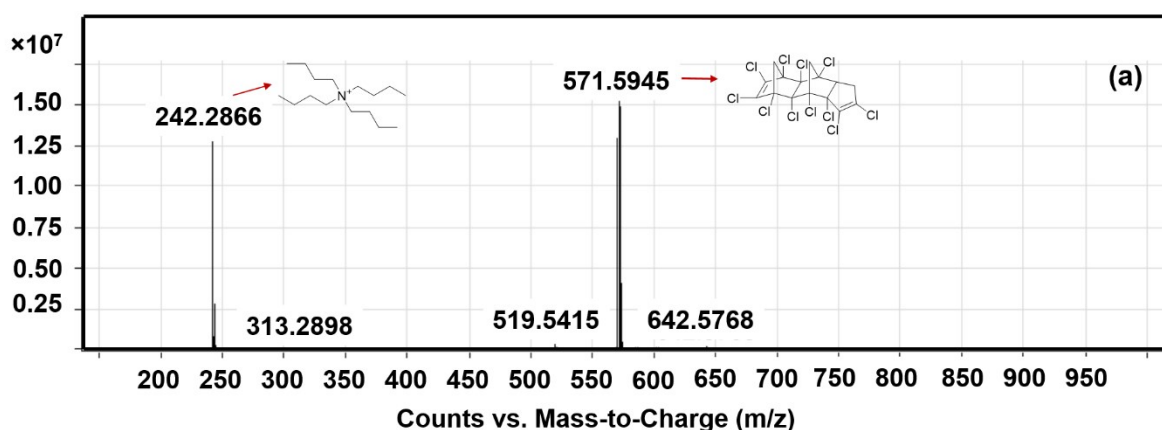
Fig. S4 Q-TOF LC/MS analysis of the electrolysis solutions of HCCP and its possible reaction products. Potential-controlled electrolysis experiments were performed at (a) -0.7 V and (b) -2.9 V vs. Ag/AgCl/KCl (3.0 M) in acetonitrile solution containing 2 mM HCCP and 0.1 M TBABF$_4$.

On the basis of the experimental results, it appears that the first step of the electrochemical reduction process is addition of four electrons to HCCP followed by a concerted mechanism where the electron transfer and the C-Cl bond dissociation are simultaneous (Scheme S1). The concerted decomposition leads to the formation of the corresponding dianion and chloride ions. The produced dianion is rapidly protonated by residual water or some other proton sources to form the final product TCCP. The diene TCCP is an excellent cyclic diene for Diels-Alder reaction with dienophiles, and thus it reacts with itself (or with HCCP or its different reduction states such as trichlorocyclopentadiene, dichlorocyclopentadiene and cyclopentadiene) to produce norbornene derivatives. By repeating this process, the growth of the polymer film occurs on the electrode surface.
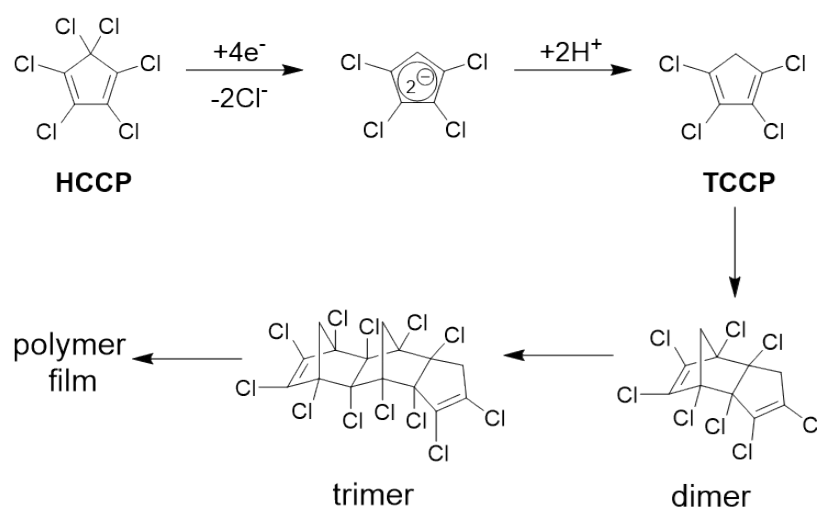
Scheme S1. Proposed reaction scheme for the electrochemical reduction of HCCP.

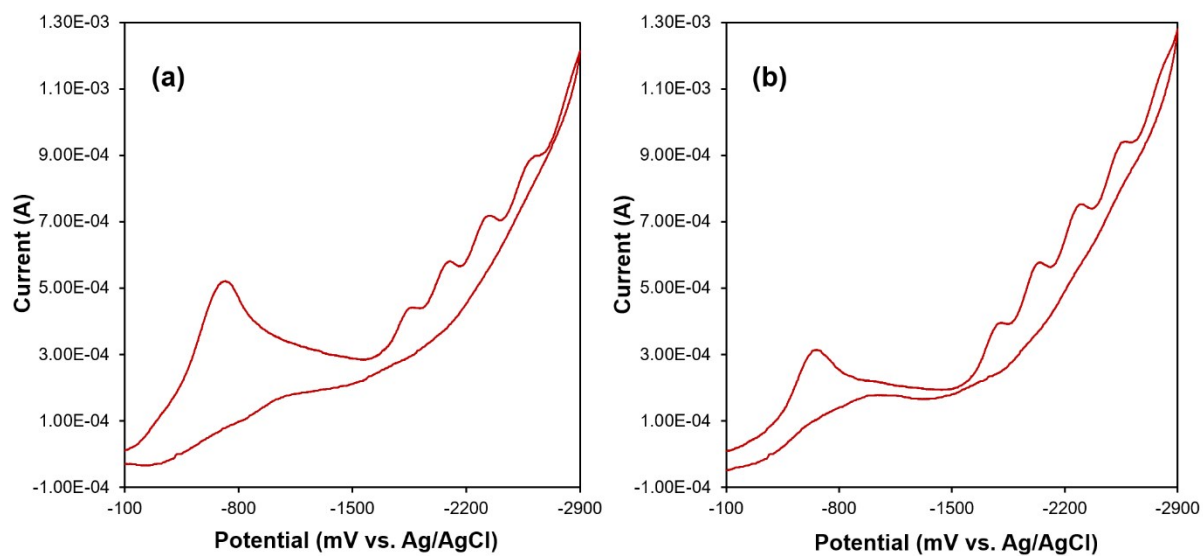## ESI2. Electrochemical Reduction of HCB/HCCP Mixtures

Fig. S5 Cyclic voltammetric responses for mixtures of HCB and HCCP at the molar ratios of (a) 2/1.2 and (b) 2/0.6 in acetonitrile containing 0.1 M TBABF$_4$ with scan rate of 0.1 V s^{-1} at gold electrodes.

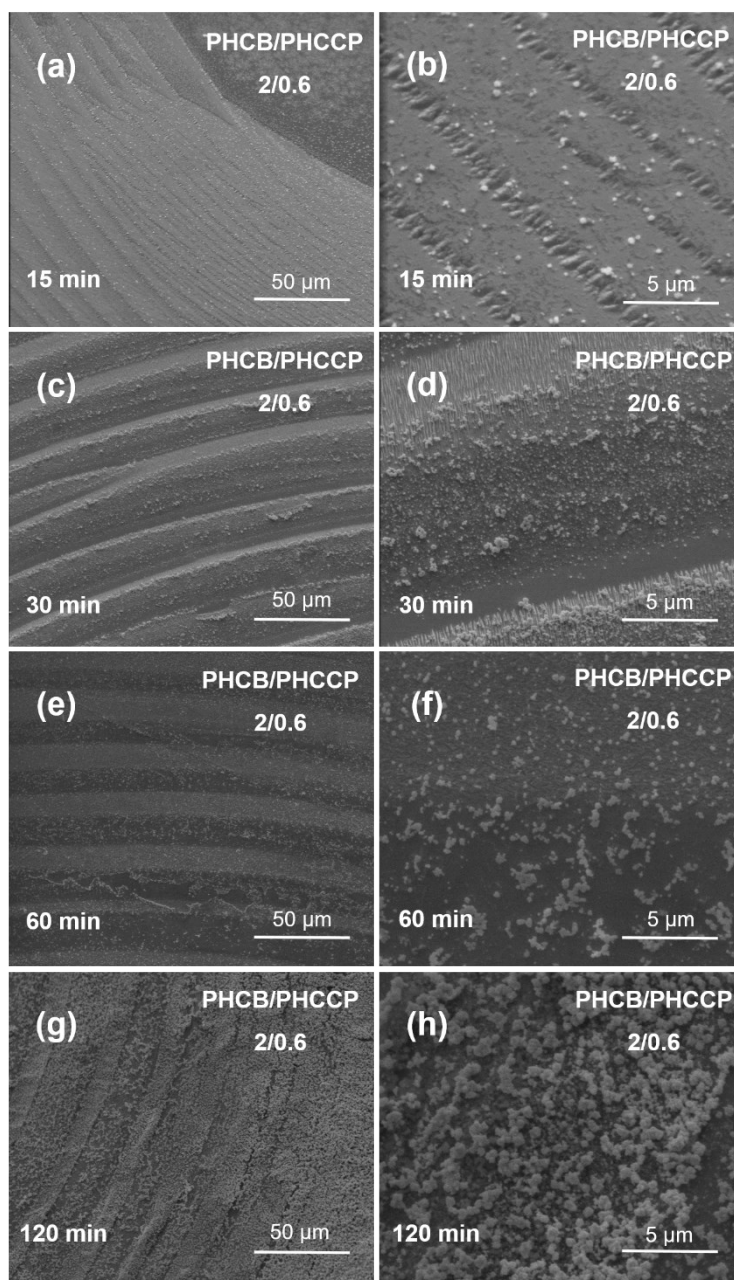**ESI3. SEM Images of PHCB/PHCCP Films**

Fig. S6 SEM images of carbon films obtained by potential-controlled electrolysis in 0.1 M TBABF$_4$/acetonitrile solution containing 2 mM HCB and 0.6 mM HCCP. For a 15 min deposition time, the small polymer particles concentrated at the step edges of the gold were observed. As the electrolysis time increases, a greater density of the larger particles was formed on the electrode surface. At the end of 120 min electrolysis, the surface was covered with irregular-shaped particles.
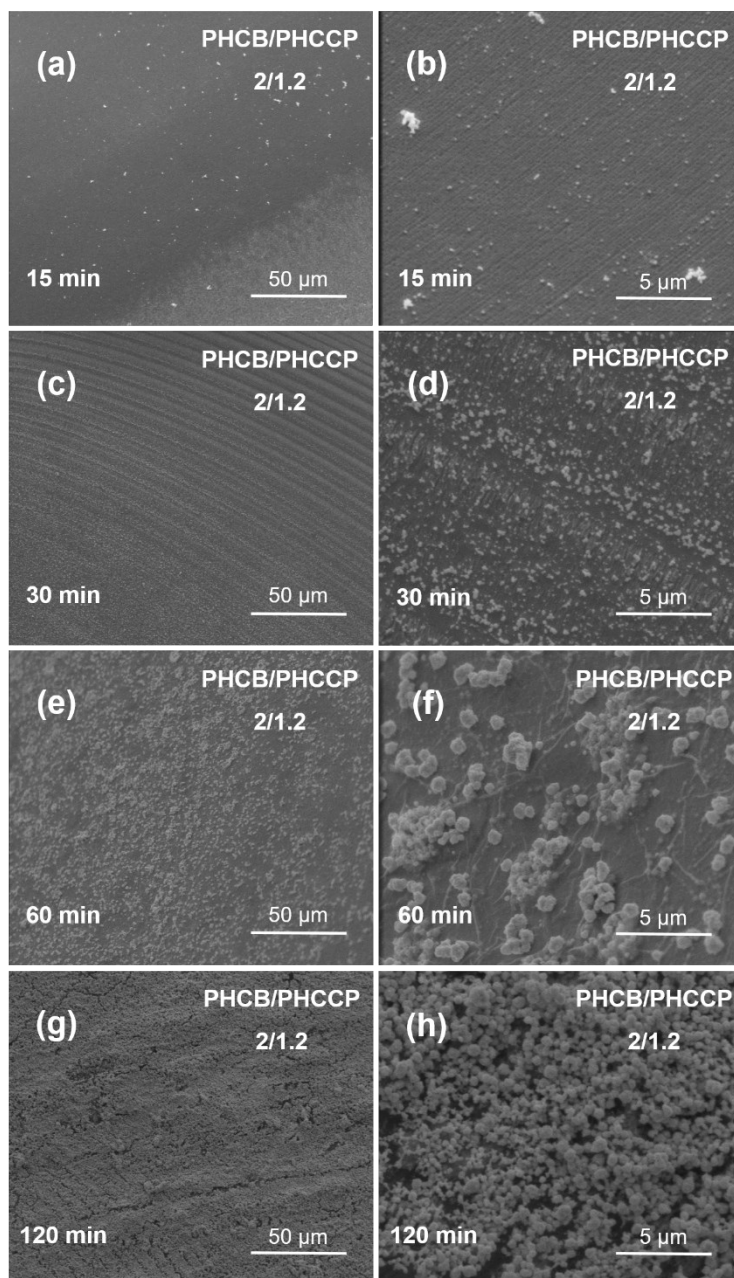
Fig. S7 SEM images of carbon films obtained by potential-controlled electrolysis in 0.1 M TBABF$_4$/acetonitrile solution containing 2 mM HCB and 1.2 mM HCCP. After 15 min of deposition, a smooth coating containing small particles was observed. With increasing electrolysis time, the particle size and density increased, and the smooth film on the electrode surface transformed to the crumpled form. At the end of 120 min electrolysis, the surface was covered with nanoflower-like carbon particles of various sizes.
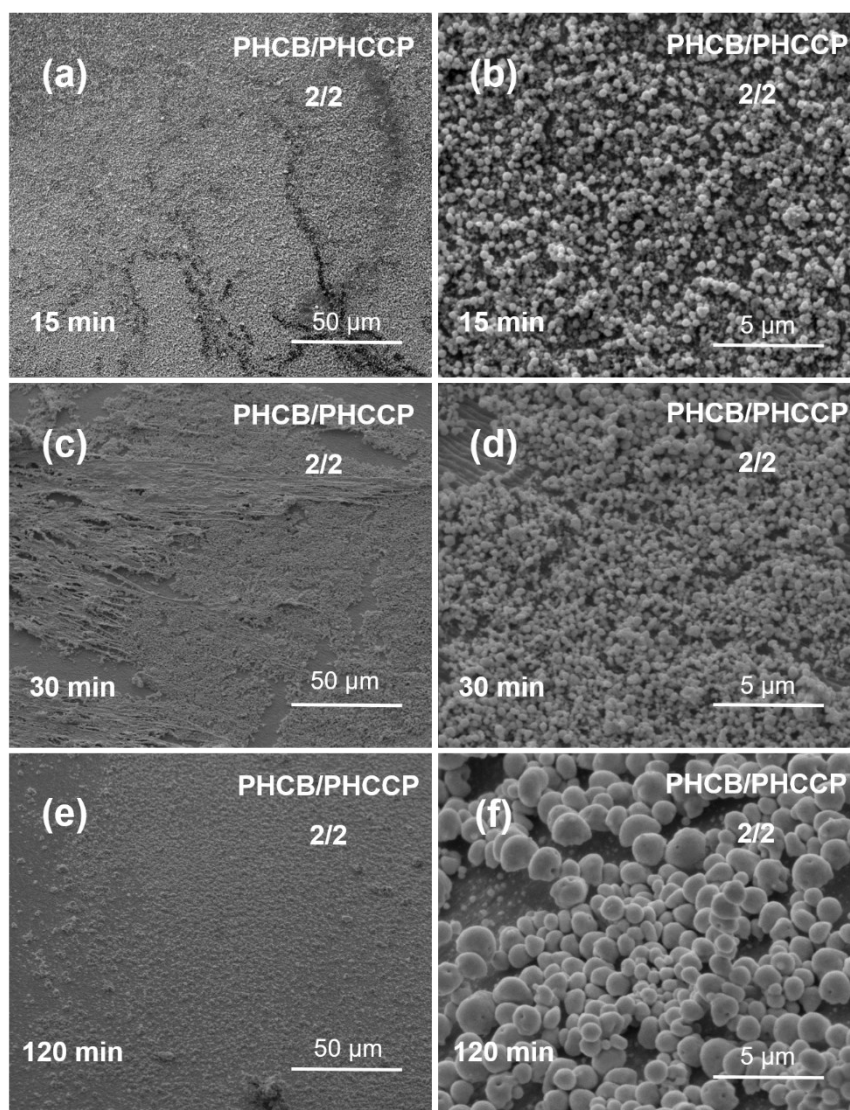

Fig. S8 SEM images of carbon films obtained by potential-controlled electrolysis in 0.1 M TBABF$_4$/acetonitrile solution containing 2 mM HCB and 2 mM HCCP. After the first 15 min of

deposition, the gold surface was densely covered with spherical particles. After 30 min of deposition, the particles gathered together, and also the presence of a laminar layer similar to that observed in the PHCCP film was obtained on the electrode surface. At the end of 120 min electrolysis, the particles transformed to the nanomushroom-like structures.
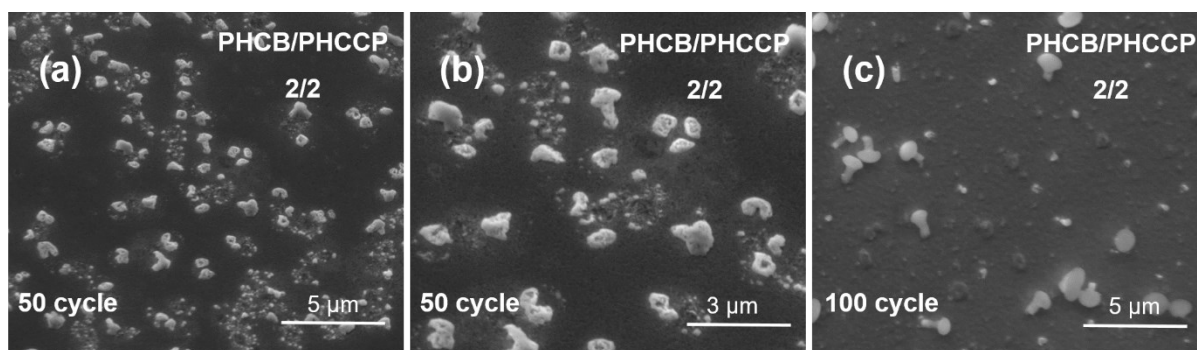

Fig. S9 SEM images of carbon films obtained by potential cycling between -0.1 and -2.9 V at a scan rate of 0.1 V s^{-1} in 0.1 M TBABF$_4$/acetonitrile solution containing 2 mM HCB and 2 mM HCCP.
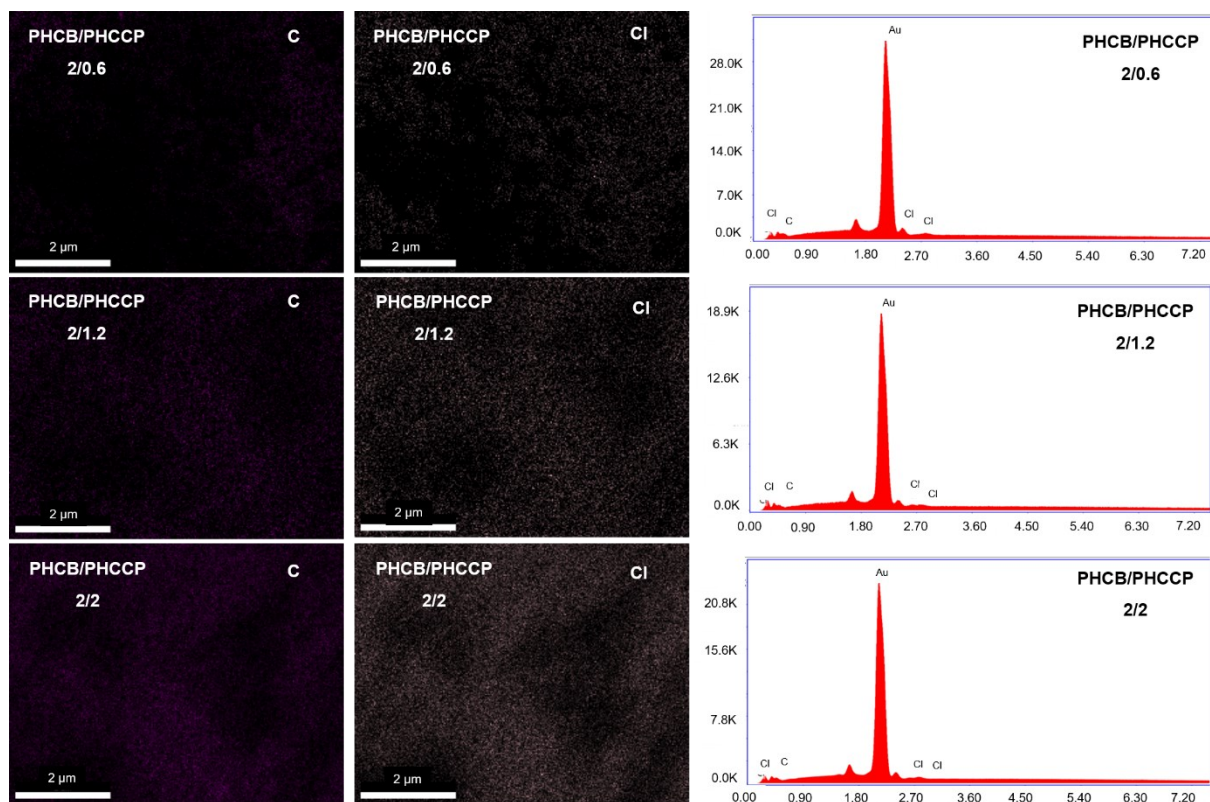
Fig. S10 SEM-EDS analyzes of carbon films on gold substrates. EDS elemental mapping images and EDS spectra of carbon films.

ESI4. XRD Analysis of Carbon Films

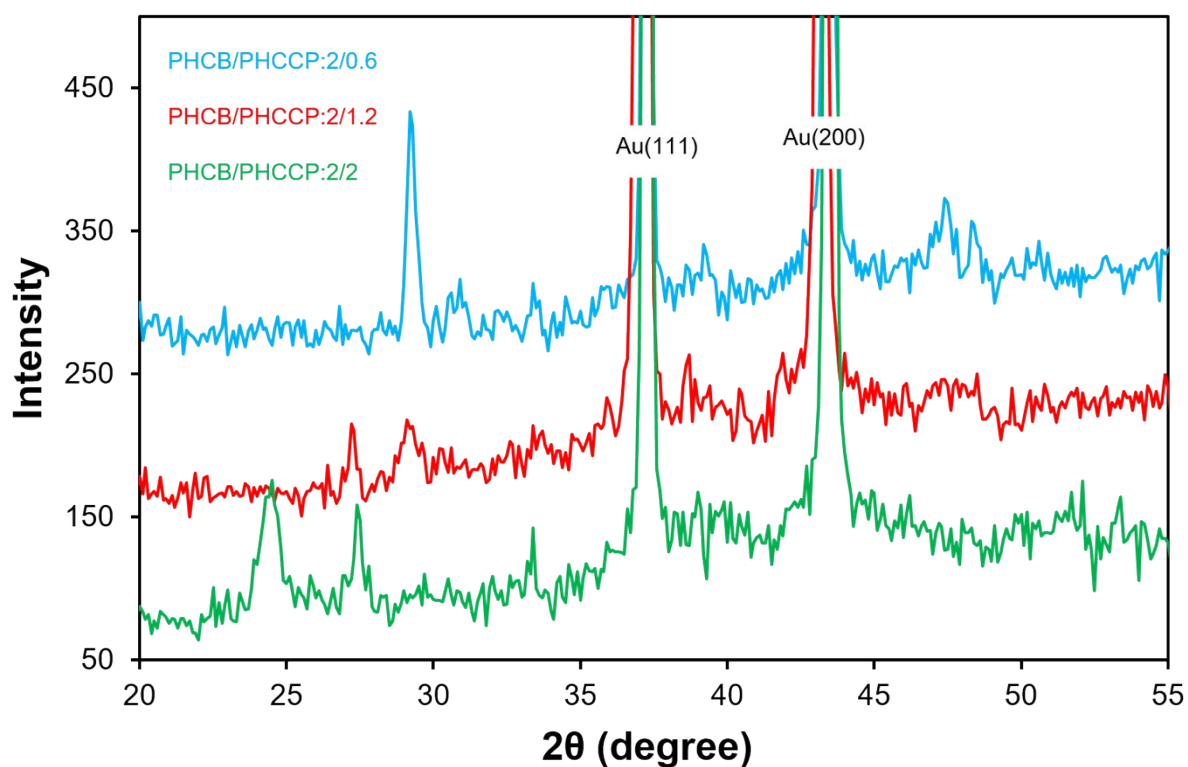**Fig. S11** XRD patterns of carbon films on gold substrates.

Table S1. XRD crystalline structure parameters of carbon films.

sample	2θ	d_{002} (nm)
PHCB/PHCCP (2/0.6)	29.2°	0.306
PHCB/PHCCP (2/1.2)	29.1° and 27.3°	0.306 and 0.326
PHCB/PHCCP (2/2)	27.4° and 24.5°	0.325 and 0.363

ESI5. XPS Analysis of Carbon Films

Table S2. XPS analysis parameters obtained from the C1s spectra.

| sample		Csp^2	Csp^3	C-Cl
PHCB	peak center (eV)	283.5	284.8	286.9
	fwhm	1.73	1.88	2.19
	atomic%	39.42	33.24	27.35
THCB	peak center (eV)	283.9	285.1	287.5
	fwhm	1.47	1.89	1.87
	atomic%	64.05	25.07	10.87
PHCCP	peak center (eV)	284.1	285.4	287.1
	fwhm	1.75	1.80	1.94
	atomic%	38.91	41.56	19.54
THCCP	peak center (eV)	284.0	285.3	287.2
	fwhm	1.53	1.76	1.91
	atomic%	54.64	32.92	12.43
PHCB/PHCCP (2/0.6)	peak center (eV)	283.8	285.5	286.6
	fwhm	2.06	1.54	1.68
	atomic%	54.76	27.07	18.18
THCB/THCCP (2/0.6)	peak center (eV)	283.9	285.0	286.6
	fwhm	1.44	1.62	1.44
	atomic%	57.68	32.39	9.92
PHCB/PHCCP (2/1.2)	peak center (eV)	283.7	285.1	286.8
	fwhm	1.82	1.82	1.82
	atomic%	54.13	31.13	14.74
THCB/THCCP (2/1.2)	peak center (eV)	284.2	285.5	287.3
	fwhm	1.44	1.80	1.66
	atomic%	57.09	31.13	11.77
PHCB/PHCCP (2/2)	peak center (eV)	283.4	285.0	286.6
	fwhm	1.88	1.78	1.65
	atomic%	60.93	27.92	11.15
THCB/THCCP (2/2)	peak center (eV)	283.9	285.4	287.6
	fwhm	1.52	1.82	1.90
	atomic%	70.59	20.50	8.90
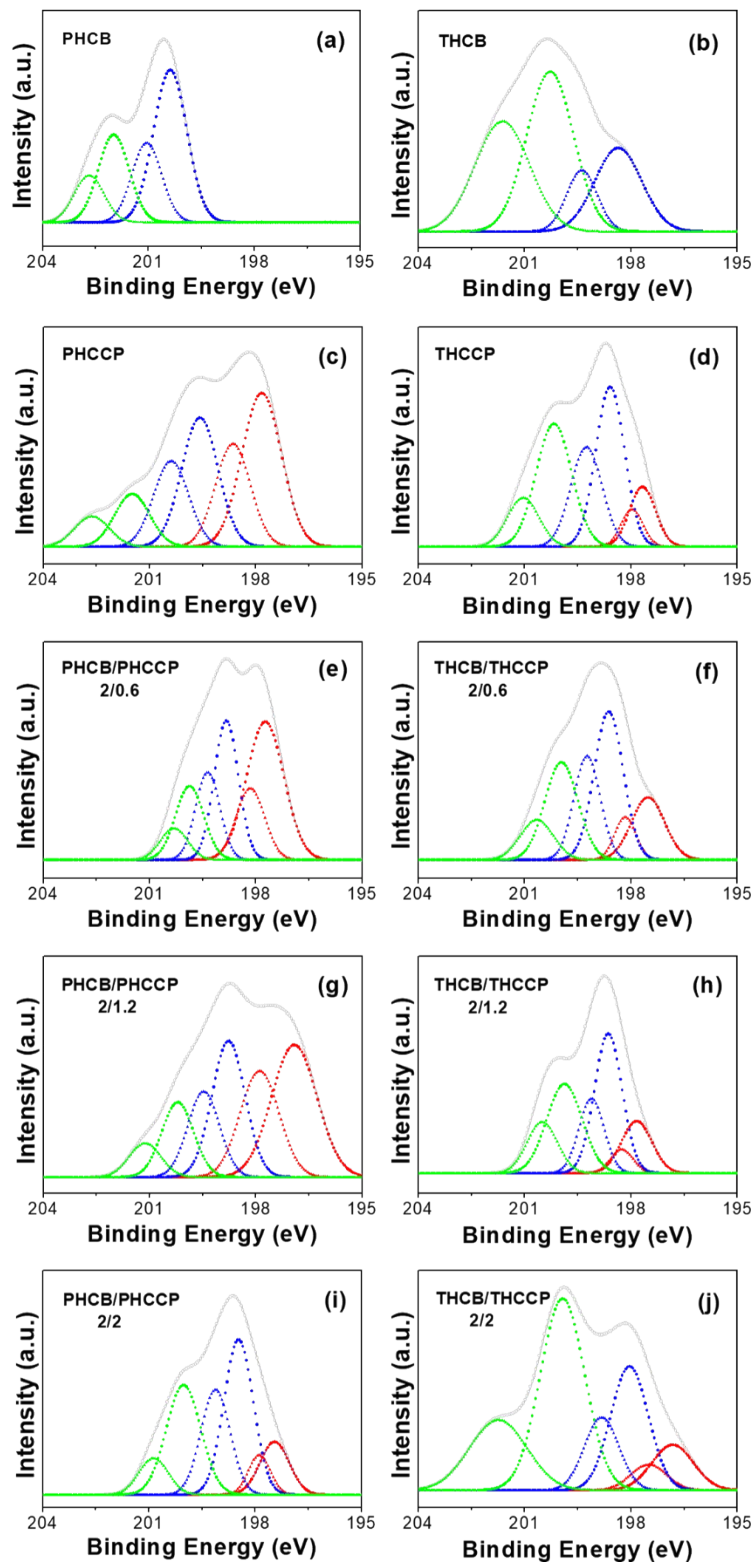
Fig. S12 Deconvoluted Cl2p XPS spectra of carbon films deposited by 120 min electrolysis before and after annealing at 400 ^{0}C.

Table S3. XPS analysis parameters obtained from the Cl2p spectra.

sample		Cl2p$_{3/2}$ (C-Cl$_2$)	Cl2p$_{1/2}$ (C-Cl$_2$)	Cl2p$_{3/2}$ (Csp^3–Cl)	Cl2p$_{1/2}$ (Csp^3–Cl)	Cl2p$_{3/2}$ (Csp^2-Cl)	Cl2p$_{1/2}$ (Csp^2-Cl)
PHCB	peak center (eV)	-	-	200.4	201.0	201.9	202.7
	fwhm	-	-	1.11	0.99	1.03	0.99
	atomic%	-		64.44		35.56	
THCB	peak center (eV)	-	-	198.4	199.4	200.3	201.6
	fwhm	-	-	1.55	1.02	1.55	1.81
	atomic%	-		30.05		69.95	
PHCCP	peak center (eV)	197.8	198.6	199.6	200.4	201.5	202.6
	fwhm	1.31	1.16	1.21	1.16	1.16	1.16
	atomic%	47.65		37.99		14.35	
THCCP	peak center (eV)	197.7	197.9	198.6	199.2	200.2	201.0
	fwhm	0.86	0.72	0.95	1.04	1.18	1.04
	atomic%	14.80		48.27		36.93	
PHCB/PHCCP (2/0.6)	peak center (eV)	197.7	198.1	198.8	199.4	199.9	200.3
	fwhm	1.24	0.95	0.81	0.81	0.94	0.90
	atomic%	45.92		35.22		18.86	
THCB/THCCP (2/0.6)	peak center (eV)	197.5	198.2	198.6	199.2	199.9	200.7
	fwhm	1.09	0.71	0.96	0.87	1.09	1.09
	atomic%	20.41		48.29		31.29	
PHCB/PHCCP (2/1.2)	peak center (eV)	196.9	197.9	198.8	199.5	200.2	201.1
	fwhm	1.51	1.29	1.10	1.06	1.06	1.06
	atomic%	48.64		34.75		16.61	
THCB/THCCP (2/1.2)	peak center (eV)	197.8	198.3	198.6	199.1	199.9	200.5
	fwhm	1.00	0.75	0.91	0.83	1.18	1.00
	atomic%	16.81		45.61		37.58	
PHCB/PHCCP (2/2)	peak center (eV)	197.4	197.9	198.5	199.1	200.0	200.9
	fwhm	0.97	0.73	0.97	0.97	1.14	0.97
	atomic%	16.27		51.15		32.58	
THCB/THCCP (2/2)	peak center (eV)	196.8	197.5	198.0	198.8	199.9	201.7
	fwhm	1.38	1.19	1.24	1.14	1.47	1.89
	atomic%	12.50		31.78		55.72	

ESI6. Raman Analysis of Carbon Films

Table S4. Raman peak positions (cm^{-1}) for the carbon films.

sample	peak I	peak II	peak III	peak IV	peak V	peak VI	peak VII
PHCB	1126.6	1234.1	1288.8	1339.3	1432.9	1568.8	1623.3
THCB	1140.9	1215.9	1275.4	1344.6	1410.5/ 1467.8	1563.1	1621.0
PHCCP	1135.0	1229.0	1296.8	1361.2	1449.3	1573.1	1625.5
THCCP	1118.5	1212.0	1292.6	1366.1	1459.1	1578.4	1619.6
THCB/THCCP (2/0.6)	1014.4	1107.4	1213.5	1343.9	1459.1	1562.2	1623.1
THCB/THCCP (2/1.2)	1057.0	1144.9	1237.8	1355.2	1465.9	1568.8	1625.3
THCB/THCCP (2/2)	1074.7	1155.2	1238.0	1348.6	1466.4	1574.3	1620.5

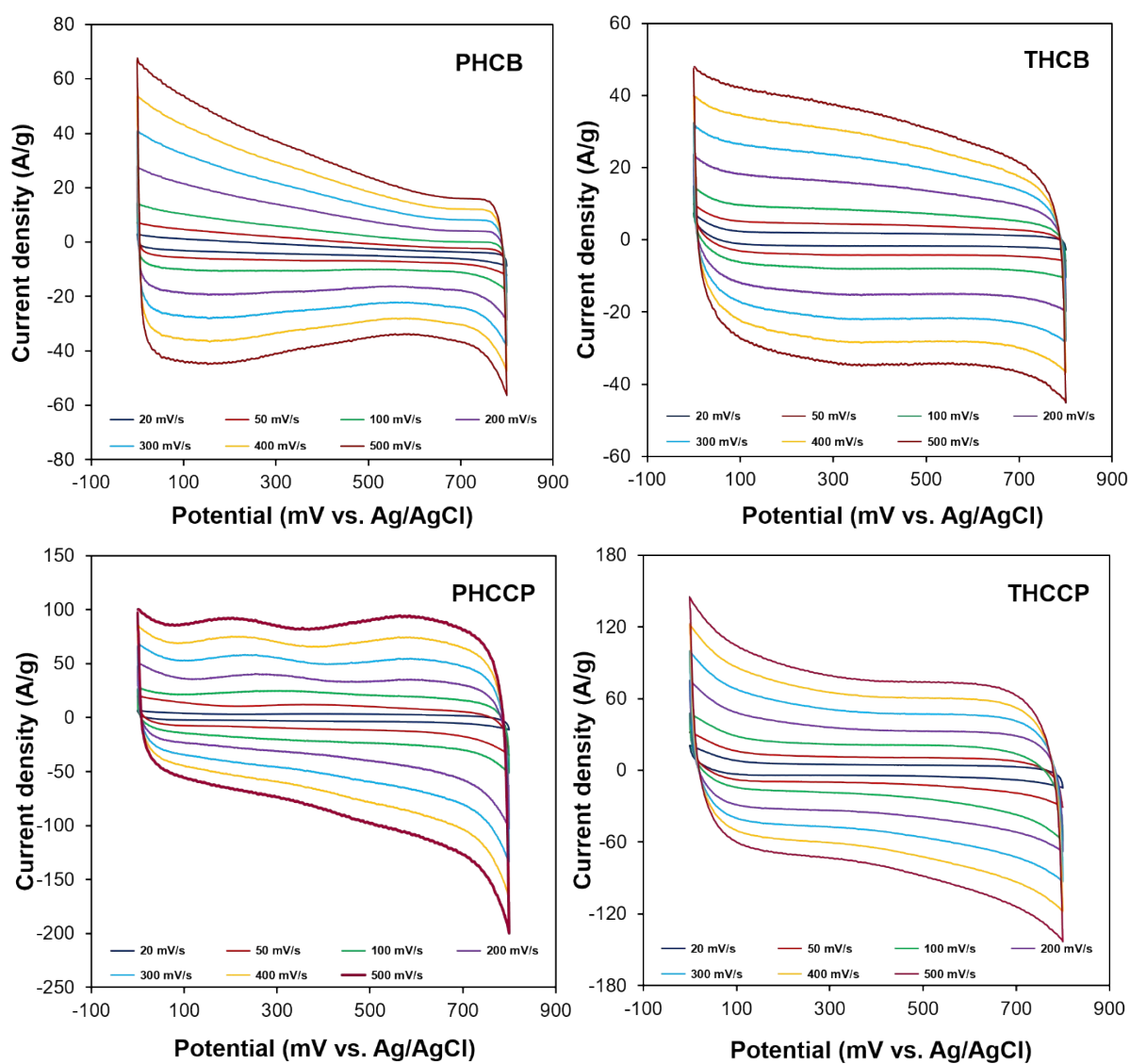## ESI7. Capacitive Performances of Carbon Films

Fig. S13 CV curves recorded for PHCB/Au, THCB/Au, PHCCP/Au and THCCP/Au electrodes in 1 M Na_2SO_4 aqueous solution at different scan rates (20 to 500 mV s^{-1}).
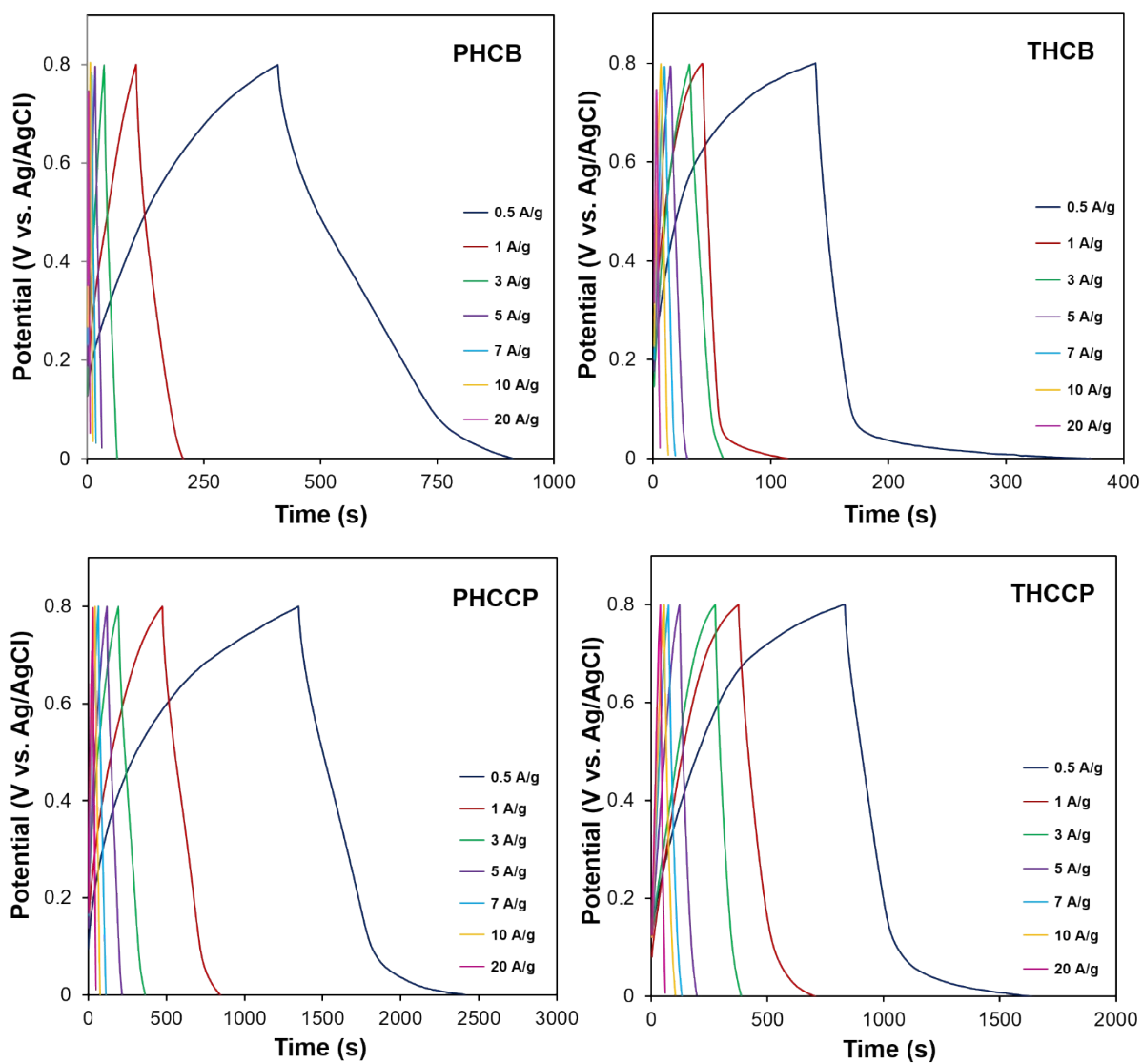
Fig. S14 GCD curves recorded for PHCB/Au, THCB/Au, PHCCP/Au and THCCP/Au electrodes in 1 M Na$_2$SO$_4$ aqueous solution at different current densities (0.5 A g^{-1} to 20 A g^{-1}).
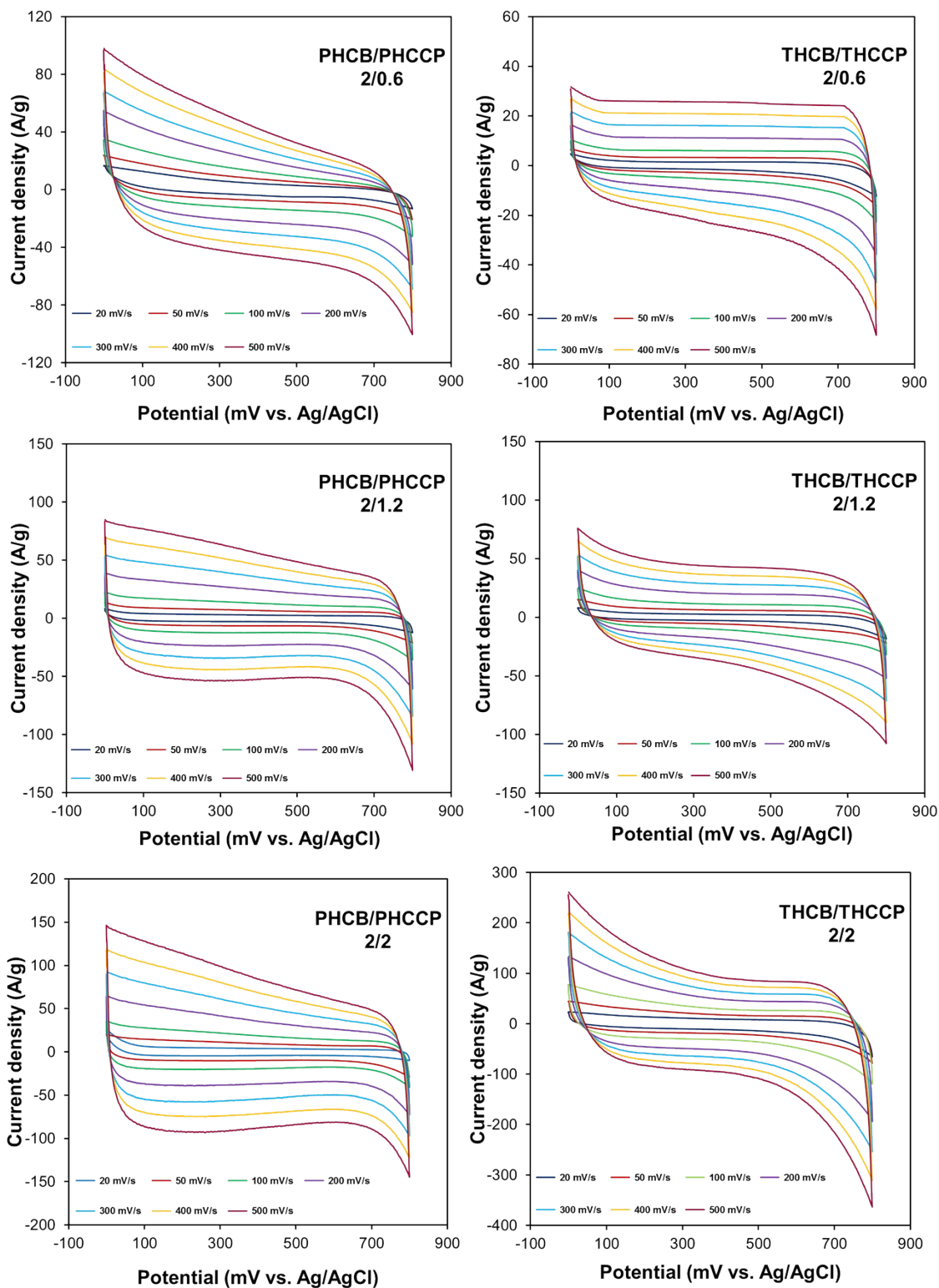
S20

Fig. S15 CV curves recorded for the carbon films in 1 M Na_2SO_4 aqueous solution at different scan rates (20 to 500 mV s^{-1}).
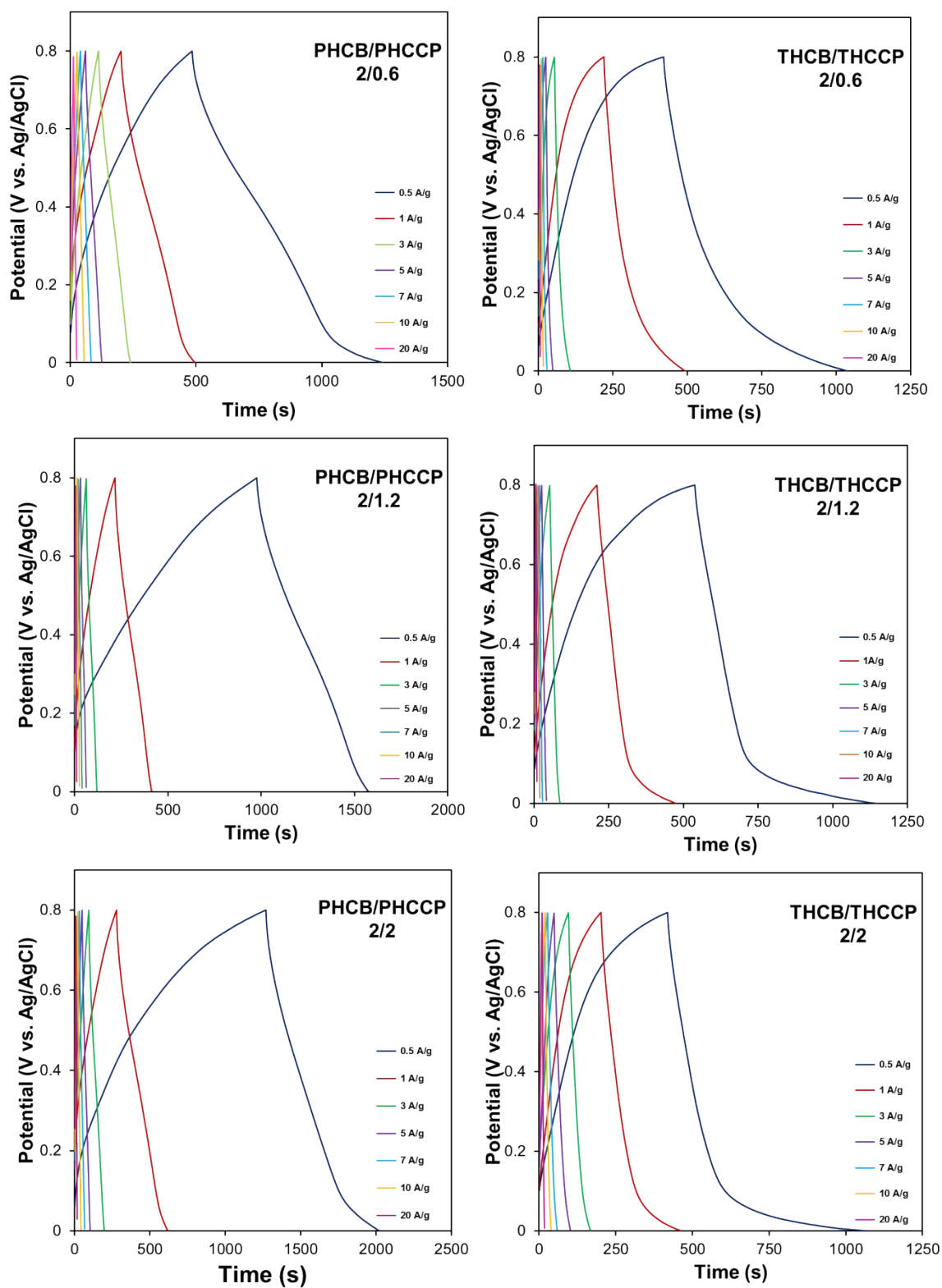
S21

Fig. S16 GCD curves recorded for the carbon films in 1 M Na_2SO_4 aqueous solution at different current densities (0.5 A g^{-1} to 20 A g^{-1}).

Table S5. The specific capacitances (C_S) of the carbon films estimated based on the results of CV and GCD measurements.

sample	C_S (F g^{-1})													
	$C_{S,CV}$ (different scan rates, mV s^{-1})							$C_{S,GCD}$ (different current density, A g^{-1})						
	20	50	100	200	300	400	500	0.5	1	3	5	7	10	20
PHCB	147.6	132.6	110.7	90.3	75.4	68.9	68.8	175.3	146.4	110.9	86.5	70.0	64.4	60.0
THCB	88.1	84.3	80.2	75.8	72.1	70.8	68.1	73.2	52.5	44.8	43.8	36.8	32.8	27.9
PHCCP	277.9	228.7	209.3	184.4	177.3	170.2	167.4	331.8	242.1	178.4	155.3	138.9	129.6	107.5
THCCP	220.6	215.1	196.6	175.3	165.4	160.8	155.9	251.8	206.4	174.5	150.4	135.5	123.3	104.1
PHCB/PHCCP (2/0.6)	157.3	140.2	120.6	105.7	95.9	90.2	87.7	182.0	175.5	100.5	81.6	74.9	65.8	52.7
THCB/THCCP (2/0.6)	102.2	86.1	81.3	67.4	55.2	51.7	49.5	192.8	171.3	93.1	75.0	61.3	50.0	31.5
PHCB/PHCCP (2/1.2)	221.1	195.0	172.9	140.8	127.4	116.4	108.5	186.9	144.4	106.8	93.7	87.5	81.2	70.0
THCB/THCCP (2/1.2)	197.5	152.5	128.9	104.6	94.6	85.1	82.3	191.3	165.6	128.8	104.3	80.0	70.8	60.5
PHCB/PHCCP (2/2)	305.9	247.3	218.1	198.3	183.9	174.5	172.0	235.0	215.5	180.7	162.8	147.0	134.7	110.7
THCB/THCCP (2/2)	306.1	274.3	251.0	218.6	202.2	193.1	185.6	201.4	178.3	156.5	133.1	129.6	115.8	93.6

Table S6. The fit values for circuit elements estimated based on the EIS measurements

sample	R_s (Ω)	R_{ct} (Ω)	Z_W (Ω)	C_{dl} (F)	τ (ms)
PHCB	11.6	181.1	0.0015	43.2×10^{-6}	3.0
THCB	7.5	73.2	0.0051	17.6×10^{-6}	8.8
PHCCP	6.1	340.5	0.0045	79.8×10^{-6}	2.5
THCCP	7.7	364.8	0.0022	152.8×10^{-6}	8.1
PHCB/PHCCP (2/0.6)	5.2	120.6	0.06	663.6×10^{-6}	30
THCB/THCCP (2/0.6)	4.4	65.4	0.01	454.1×10^{-6}	20
PHCB/PHCCP (2/1.2)	6.6	400.2	0.05	732.2×10^{-6}	40
THCB/THCCP (2/1.2)	6.4	290.7	0.08	203.9×10^{-6}	10
PHCB/PHCCP (2/2)	7.1	137.4	0.01	577.4×10^{-6}	40
THCB/THCCP (2/2)	8.6	149.8	0.03	246.7×10^{-6}	20

Table S7. Comparison of specific capacitances of the carbon-based materials.

| precursor	material structure	synthesis conditions	electrolyte	test condition (A g^{-1})	specific capacitance (F g^{-1})	Ref
bio waste	porous carbon	H_3PO_4 activation and carbonization at 900 °C	1 M Na_2SO_4	1	320	15
polystyrene	mesoporous graphene nanoballs	precursor assisted CVD	1 M H_2SO_4	1	206	16
polyimide	nitrogen-doped holey carbon nanosheets	template assisted carbonization at 900 °C	2 M KOH	0.5	205	17
glucose	RGO wrapped nitrogen-doped carbon nanoflowers	hydrothermal treatment at 800 °C and freeze drying method	6 M KOH	0.5	344	18
polyaniline	activated carbon nanosheets	carbonization at 800 °C and activation process	1 M H_2SO_4	1	315	19
PHCCP	carbon nanosheets	electrochemical reduction	1 M Na_2SO_4	0.5	331	this study
PHCB/PHCCP (2/2)	carbon nanomushrooms	electrochemical reduction	1 M Na_2SO_4	0.5	235	this study
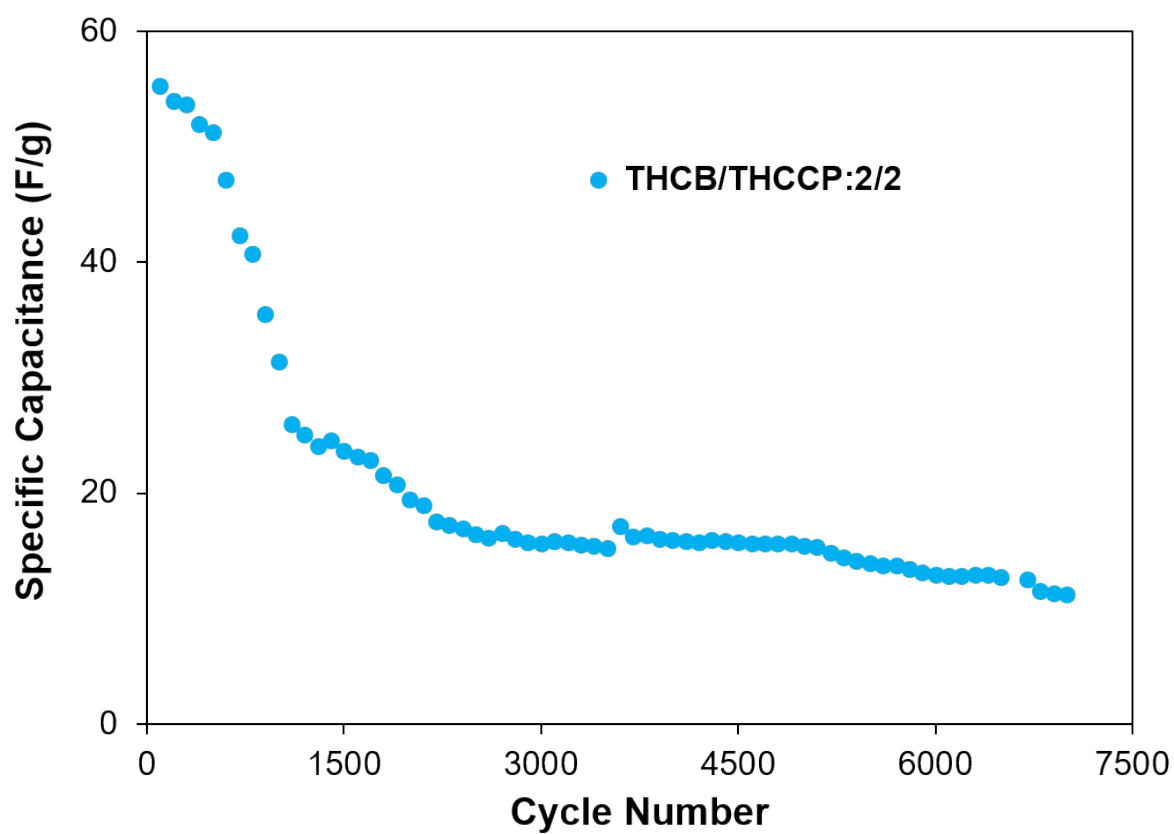
Fig. S17 For THCB/THCCP:2/2 electrode variation of specific capacitances with cycle number.

ESI8. Surface Area and Porosity Characteristics of Carbon films

Table S8. Surface area and porosity characteristics of carbon films

sample	BET specific surface area ($m^2 g^{-1}$)	total pore volume ($cm^3 g^{-1}$)	surface area of pores >1.7 nm ($m^2 g^{-1}$)
PHCB/PHCCP (2/0.6)	1242	1.29	642.7
PHCB/PHCCP (2/1.2)	1454	1.07	560.2
PHCB/PHCCP (2/2)	1955	1.21	935.1

ESI9. References

1   A. A. Ordaz, J. M. Rocha, F. J. A. Aguilar, S. G. Granados, F. Bedioui, *Analusis*, 2000, **28**, 238-244.

2   Z. Kudaş, E. Gür, D. Ekinci, *Langmuir*, 2018, **34**, 7958-7970.

3   A. Isse, S. Gottardello, C. Durante, A. Gennaro, *Phys. Chem. Chem. Phys.* 2008, **10**, 2409-2416.

4   A. Isse, G. Sandonà, C. Durante, A. Gennaro, *Electrochim. Acta*, 2009, **54**, 3235-3243.

5   A. Muthukrishnan, V. Boyarskiy, M. V. Sangaranarayanan, I. Boyarskaya, *J. Phys. Chem. C*, 2012, **116**, 655-664.

6   F. C. Anson, *Anal. Chem.*, 1964, **36**, 932-934.

7   E. T. McBee, R. K. Meyers, C. F. Baranauckas, *J. Am. Chem. Soc.*, 1955, **77**, 86-88.

8   E. T. McBee, D. K. Smith, *J. Am. Chem Soc.*, 1955, **77**, 389-391.

9   E. T. McBee, J. D. Idol Jr., C. W. Roberts, *J. Am. Chem. Soc.*, 1955, **77**, 4375-4379.

10 A. Roedig, L. Hörnig, *Angew. Chem.*, 1955, **67**, 302-300.

11 D. Robb, M. W. Blades, *J. Am. Soc. Mass Spectrom.*, 1997, **8**, 1203-1205.

12 G. A. Tolstikov, S. A. Ismailov, F. A. Gimalova, N. A. Ivanova, M. S. Miftakhov, *Russ. Chem. Bull., Int. Ed.*, 2013, **62**, 226-234.

13 R. S. Pavelyev, R. M. Vafina, O. A. Lodochnikova, A. S. Galiullina, E. I. Romanova, K. V. Balakin, Y. G. Shtyrlin, *Tetrahedron Lett.*, 2016, **57**, 3902-3907.

14 B. V. Lap, M. N. Paddon-Row, *J. Org. Chem.*, 1979, **44**, 4979-4981.

15 R. J. Ramalingam, M. Sivachidambaram, J. J. Vijaya, H. A. Al-Lohedan, M. R. Muthumareeswaran, *Biomass and Bioenergy*, 2020, **142**, 105800.

16 J.-S. Lee, S.-I. Kim, J.-C. Yoon, J.-H. Jang, *ACS Nano*, 2013, **7**, 6047.

17 H. Peng, S. Qi. Q. Miao, R. Zhao, Y. Xu, G. Ma, Z. Lei, *J. Power Sources*, 2021, **482**, 228993.

18 F. Ding, Z. Yu, X. Chen, X. Chen, C. Chen, Y. Huang, Z. Yang, C. Zou, K. Yang, S. Huang, *Electrochim. Acta*, 2019, **306**, 549.

19 W. Chen, R. B. Rakhi, M. N. Hedhili, H. N. Alshareef, *J. Mater. Chem. A*, 2014, **2**, 5236.